

MIT Open Access Articles

Substantial reduction of Stone-Wales activation barrier in fullerene

The MIT Faculty has made this article openly available. **Please share** how this access benefits you. Your story matters.

Citation: Kabir, Mukul, Swarnakamal Mukherjee, and Tanusri Saha-Dasgupta. "Substantial Reduction of Stone-Wales Activation Barrier in Fullerene." *Physical Review B* 84.20 (2011): [7 pages]. ©2011 American Physical Society.

As Published: <http://dx.doi.org/10.1103/PhysRevB.84.205404>

Publisher: American Physical Society

Persistent URL: <http://hdl.handle.net/1721.1/69964>

Version: Final published version: final published article, as it appeared in a journal, conference proceedings, or other formally published context

Terms of Use: Article is made available in accordance with the publisher's policy and may be subject to US copyright law. Please refer to the publisher's site for terms of use.



Substantial reduction of Stone-Wales activation barrier in fullerene

Mukul Kabir,^{1,*} Swarnakamal Mukherjee,² and Tanusri Saha-Dasgupta²

¹*Department of Materials Science and Engineering, Massachusetts Institute of Technology, Cambridge, Massachusetts 02139, USA*

²*Advanced Materials Research Unit and Department of Material Sciences, S.N. Bose National Center for Basic Sciences, JD Block, Sector III, Salt Lake City, Kolkata 700 098, India*

(Received 11 May 2011; revised manuscript received 11 October 2011; published 10 November 2011)

Stone-Wales (SW) transformation is a key mechanism responsible for the growth, transformation, and fusion in fullerenes, carbon nanotubes, and other carbon nanostructures. These topological defects also substantially alter the physical and chemical properties of the carbon nanostructures. However, this transformation is thermodynamically limited by very high activation energy (~ 7 eV in fullerenes). Using first-principles density functional calculations, we show that the substitutional boron doping substantially reduces the SW activation barrier (from ~ 7 to 2.54 eV). This reduction is the largest in magnitude among all the mechanisms of barrier reduction reported to date. Analysis of bonding charge density and phonon frequencies suggests that the bond weakening at and around the active SW site in B heterofullerenes is responsible for such a reduction. Therefore, the formation of the SW defect is promoted in such heterofullerenes and is expected to affect their proposed H_2 storage properties. Such substitutional doping also can modify the SW activation barrier in carbon nanotubes and graphene nanostructures and can catalyze isomerization, fusion, and nanowelding processes.

DOI: [10.1103/PhysRevB.84.205404](https://doi.org/10.1103/PhysRevB.84.205404)

PACS number(s): 61.48.-c, 81.05.ub, 34.10.+x

I. INTRODUCTION

Stone-Wales (SW) defects¹ are important topological defects in sp^2 -bonded carbon materials, which play crucial roles in the growth, isomerism, and nanoscale plasticity of carbon nanotubes, fullerenes, and graphitic nanostructures.²⁻⁴ SW transformation involves an in-plane 90° -bond rotation with respect to the bond center. This leads to pentagon-heptagon defects (5-7-7-5 dislocation dipole) in carbon nanotubes and graphene³⁻⁵ and the interchange of a pair of pentagonal and hexagonal rings in fullerenes.¹ Such structural transformation is believed to be the fundamental unit process for the coalescence of fullerenes⁶ and nanotubes,⁷ the formation of molecular junctions for nanoelectronic devices,⁸ and plastic deformation.³ Both chemically modified and unmodified SW defects induce local curvature to the otherwise planar graphitic materials,⁹⁻¹² which may enhance the formation of nanotubes and fullerenes from planar carbon nanostructures.¹³ Also, the coalescence of fullerenes and nanotubes has been proposed to occur through a sequence of such structural transformations.^{6,7} SW defects also alter the electronic properties of carbon nanostructures, and thus, substantially modify chemical reactivity toward adsorbates (reactivity increases compared to the pristine counterpart)¹⁴⁻¹⁷ and transport properties.^{18,19} Also, similar SW defects are observed in boron nitride nanotubes and nanosheets^{5,20} and are found to have important implications in determining the physical and chemical properties.²¹

It is known that 94% of the C_{60} isomers can be derived by a sequence of SW bond rotations.²² Thus, SW transformation is believed to be the fundamental mechanism for fullerene isomerism or I_h - C_{60} formation, which is the global minimum on the complex potential energy surface.^{23,24} Interchange of a pair of pentagonal and hexagonal rings in I_h - C_{60} via a single SW transition leads to C_{2v} symmetry, which does not obey the isolated-pentagon rule.²⁵ This is the first isomer, and it is separated by ~ 1.6 -eV energy from the global I_h minimum.²⁶⁻²⁸ Therefore, C_{2v} - C_{60} represents the first step toward fullerene isomerism or the last step of the annealing

process before reaching the icosahedral global minimum.²³ Although earlier, the pristine C_{2v} isomer was not observed experimentally, recently, the chlorinated C_{2v} isomer was stabilized experimentally via Krätschmer-Huffman synthesis²⁹ and in the gas phase by subsequent dechlorination.³⁰ However, the SW transition in fullerenes is thermodynamically limited due to a very large activation barrier (~ 7 eV, Fig. 1).^{27,31,32} This energy barrier is reduced in the presence of an extra carbon or hydrogen atom.^{2,33} The extra carbon atom acts as an autocatalyst and reduces the activation energy by ~ 2 eV when preferentially placed in the regions of paired pentagons. In contrast, the endohedral metal doping (K, Ca, and La) is relatively less effective for barrier-height reduction.²⁷

Here, we report the effect of substitutional doping on an SW transition in C_{60} through first-principles density functional calculations. We find that the activation barrier is reduced substantially by substitutional boron doping at the active SW sites. The quantitative reduction (2.12 and 4.34 eV for single and double B doping, respectively) is much larger compared to the cases with an extra carbon or hydrogen or endohedral metal doping.^{2,27,33} Boron-doped heterofullerenes ($C_{60-x}B_x$, $x \leq 6$) have been synthesized successfully³⁴ and are believed to be a promising candidate for hydrogen storage.^{35,36} It has been shown that H_2 adsorption energy increases substantially for B heterofullerenes where the B centers act as adsorption centers. The present paper shows that the formation of SW defects is promoted in such B-doped heterofullerenes, which may alter the reversible storage properties as SW defects are known to be more reactive toward adsorbates. Also, the presence of such a substitutional dopant is expected to reduce the activation barrier and to promote SW transition in other carbon nanostructures, and thus, to catalyze isomerism, fusion, and nanowelding processes.

II. METHODOLOGY

Calculations were carried out using density functional theory (DFT) implemented in the Vienna *ab initio*

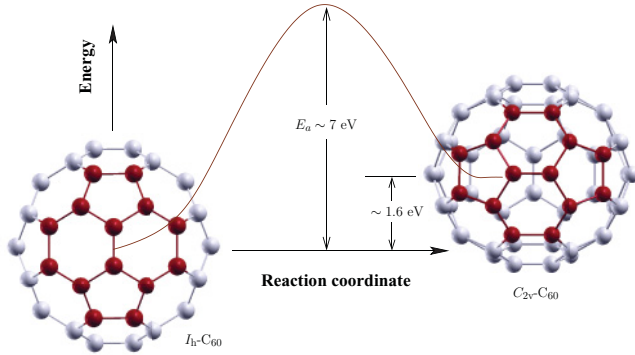


FIG. 1. (Color online) The activation energy barrier E_a for the I_h - $C_{60} \rightarrow C_{2v}$ - C_{60} transition, which represents a single SW transition, is very high. The activation barrier for the reverse transition (C_{2v} - $C_{60} \rightarrow I_h$ - C_{60}) is smaller by ~ 1.6 eV, which is the energy difference between I_h and C_{2v} symmetries. The pyracyclene region is highlighted (red).

simulation package³⁷ with the projector augmented wave pseudopotential.³⁸ If not otherwise stated, we used the Perdew-Burke-Ernzerhof (PBE) exchange-correlation functional,³⁹ and non-spin-polarized calculations were performed. The kinetic-energy cutoff was chosen to be 800 eV. Symmetry unrestricted geometry optimizations were terminated when the force on each atom was less than 0.005 eV/Å. Reciprocal space integrations were carried out at the Γ point. We determined the minimum-energy path for SW transition and the corresponding migration energy barrier E_a using the climbing-image nudged elastic band (NEB) method.⁴⁰ In NEB, a set of intermediate states (images) is distributed along the reaction path connecting optimized initial and final states. To ensure the continuity of the reaction path, the images are coupled with elastic forces, and each intermediate state is fully relaxed in the hyperspace perpendicular to the reaction coordinate.

III. RESULTS AND DISCUSSIONS

Determination of the activation energy necessary for SW transition ($I_h \rightleftharpoons C_{2v}$) via the climbing-image NEB method requires structural information of the initial and final structures within the concerned level of theory. Therefore, before we discuss the effect of B doping on the SW activation barrier, we begin our discussion with the geometric and electronic properties of C_{60} , $C_{59}B$, and $C_{58}B_2$ cages.

A. C_{60} , $C_{59}B$, and $C_{58}B_2$: Structural and electronic properties

There are two types of bonds in I_h - C_{60} : [6,6] bonds (1.399 Å) at the junctions of two hexagons are smaller than [5,6] bonds (1.453 Å) at the junctions of a pentagon and a hexagon. The C_{2v} structure is the first isomer, and in agreement with previous theoretical reports,^{26–28,32} we find that this structure is 1.57 -eV higher in energy compared to the global I_h minimum. The optimized C_{60} geometries for both I_h and C_{2v} symmetries are shown in Fig. 1, and a 14-atom pyracyclene region containing the rotating C_2 dimer is shown in Fig. 2(a). Calculated^{5,6}- and⁶-bond lengths [Fig. 2(a)] are in excellent agreement with previous theoretical calculations^{32,41} and experimental measurements^{42–45} for I_h - C_{60} . The rotating

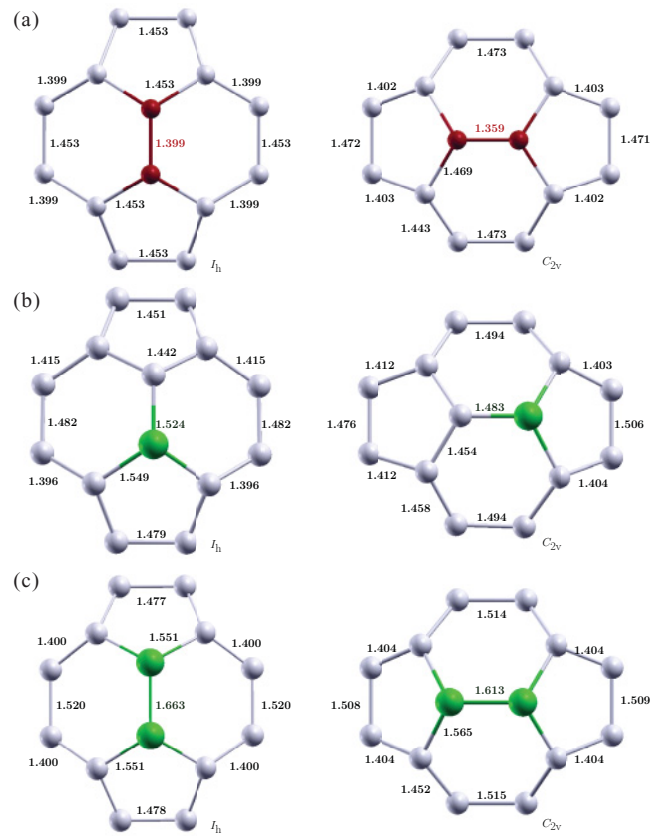


FIG. 2. (Color online) Local pyracyclene region for the optimized (a) C_{60} , (b) $C_{59}B$, and (c) $C_{58}B_2$ in I_h and C_{2v} symmetries. The rotating dimer corresponding to the SW transition is highlighted for C_{60} . The bond lengths are shown in angstroms. The length of the rotating bond decreases substantially in the C_{2v} structure for all the cages. Boron doping induces a significant local strain in $C_{59}B$, and $C_{58}B_2$ compared to pristine C_{60} .

bond in C_{2v} - C_{60} is much smaller (1.359 Å), which is also in agreement with previous theoretical calculations.^{28,32,41} However, no experimental information is available on pristine C_{2v} - C_{60} ; chlorinated C_{2v} structure ($C_{60}Cl_8$) shows a similar bond shortening of the rotating dimer (1.37 Å).²⁹ Such bond shortening introduces a local strain for the C_{2v} structure, and thus, a distribution of the bond length is observed in the pyracyclene region [Fig. 2(a)].

When one of the C atoms in the rotating dimer is replaced by B, three bond lengths involving C and B are increased (two [5,6]-C-B = 1.549 Å and one [6,6]-C-B = 1.524 Å) for I_h - $C_{59}B$ [Fig. 2(b)]. This is responsible for the bond deformation in the pyracyclene region (C-C bond distribution ranges from 1.442 to 1.482 Å). The trend of the structural changes in moving from I_h - $C_{59}B$ to C_{2v} - $C_{59}B$ remains the same as observed for pristine C_{60} . The structural properties of $C_{58}B_2$ show similar qualitative behavior. The pyracyclene region is comparatively more deformed due to the presence of one B-B (1.663 Å) bond and four C-B (1.551 Å) bonds [Fig. 2(c)]. Although, strictly speaking, both I_h and C_{2v} symmetries are broken due to B doping; for simplicity, we will retain the same nomenclature throughout the paper.

Next, we briefly discuss the electronic properties. Pure C_{60} is found to be a closed-shell singlet, whereas, doped B

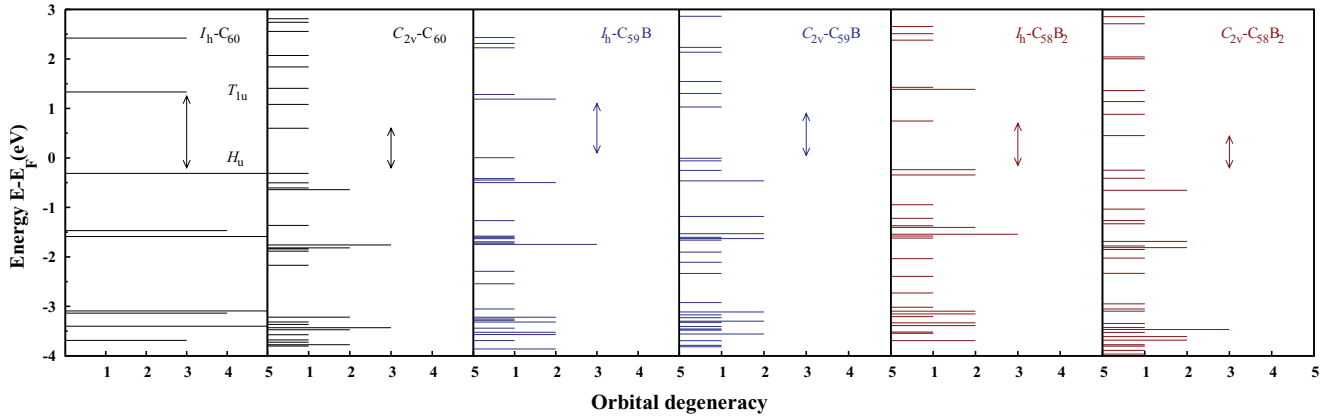


FIG. 3. (Color online) Kohn-Sham orbital degeneracy for pristine and substitutional B-doped fullerenes ($C_{59}B$ and $C_{58}B_2$) for both I_h and C_{2v} symmetries. The HOMO (LUMO) of the icosahedral C_{60} , H_u (T_{1u}) is fivefold (threefold) degenerate. Bottom (top) of the vertical arrow represents HOMO (LUMO). The introduction of defects, both in terms of topological defect and substitutional B, breaks the orbital degeneracy, and thus, reduces the Kohn-Sham energy gap E_g (see Table I).

introduces a hole (one/B doping) into the system. We note that, for $C_{59}B$, spin-polarized calculation lowers the total energy by 80 meV with respect to the non-spin-polarized calculation and yields a doublet state. In contrast, the $C_{58}B_2$ is a singlet, whereas, the triplet state lies significantly higher in energy.

The calculated Kohn-Sham energy gap between the highest occupied molecular level (HOMO) and the lowest unoccupied molecular level (LUMO) is 1.63 eV for I_h-C_{60} . Conventional density functional calculations usually underestimate the HOMO-LUMO gap obtained from the Kohn-Sham eigenvalues, which is much lower than the quasiparticle energy gap.^{46–48} For an N electron molecular system, the quasiparticle energy gap can be defined as the difference between the ionization potential ($IP = E[N-1] - E[N]$) and the electron affinity ($EA = E[N] - E[N+1]$). Here, $E[N]$ is the DFT total energy of a neutral system of N electrons. Our DFT-PBE calculations predict the IP and EA to be 7.32 and 2.75 eV, respectively, in agreement with previous DFT calculations.⁴⁹ These results, and thus, the quasiparticle gap (4.57 eV) also agree well with the self-consistent GW calculations ($IP = 7.41$ eV and $EA = 2.51$ eV)⁴⁶ and experimental measurements [$IP = 7.54 \pm 0.04$ eV (Ref. 47) and $EA = 2.65 \pm 0.05$ eV (Ref. 48)]. B heterofullerenes have somewhat smaller IP and bigger EA compared with C_{60} (Table I). These suggest that the formation of both cations and anions is relatively easier for B heterofullerenes, which indicate their enhanced redox characteristics.

Due to icosahedral symmetry, the Kohn-Sham HOMO (H_u) and LUMO (T_{1u}) are five- and threefold degenerate,

TABLE I. Energy difference between the structures in I_h and C_{2v} symmetries, $\Delta E = E(I_h) - E(C_{2v})$, and the Kohn-Sham HOMO-LUMO gap E_g . Calculated ionization potential and electron affinity for I_h symmetry. All the energies are in eV.

	ΔE	$E_g(I_h)$	$E_g(C_{2v})$	$IP(I_h)$	$EA(I_h)$
Pristine- C_{60}	1.57	1.63	0.91	7.32	2.75
$C_{59}B$	1.67	1.18	1.04	7.00	3.71
$C_{58}B_2$	1.75	0.98	0.70	7.21	3.27

respectively, for I_h-C_{60} . These degeneracies are lifted (Fig. 3) due to the presence of (1) a topological defect introduced by the SW transition and (2) substitutional B doping. Both cause a reduction in the HOMO-LUMO gap (Table I). For pristine $C_{2v}-C_{60}$, the degeneracy of both the HOMO and the LUMO is completely broken (Fig. 3), and the HOMO-LUMO gap is reduced by ~ 0.7 eV (Table I).

Substitutional B introduces a significant bond deformation in the pyracylene region [Figs. 2(b) and 2(c)], and thus, the inherent structural symmetries are broken. This removes the degeneracies of HOMO and LUMO levels (Fig. 3) and reduces the Kohn-Sham HOMO-LUMO energy gap (Table I). With subsequent B doping, the structural deformation increases [Figs. 2(b) and 2(c)], and thus, the energy gap decreases (Table I). Similarly, the presence of the SW defect further lifts the degeneracy (Fig. 3), and the gap is lower in the corresponding C_{2v} structures compared to the I_h heterofullerenes (Table I).

B. Activation barrier: Effect of substitutional B doping

Activation barriers for the SW transition in carbon nanotubes, graphitic nanostructures, and fullerenes are generally very high.^{28,50,51} Our calculated energy barrier for pristine C_{60} is found to be 6.88 eV (Table II), which is in agreement with previous reports obtained within a range of theories.^{2,27,28,32}

TABLE II. Although the activation barrier is underestimated in the PBE functional compared to the hybrid Hyed-Scuseria-Ernzerhof screened hybrid functional (HSE06), they show a similar qualitative trend. $\delta E_a [= E_a(C_{60}) - E_a(X)]$ is the reduction in the activation barrier compared to pristine C_{60} .

	Activation barrier (eV)		δE_a (eV)
	PBE	HSE06	
C_{60}	6.88	7.61	
C_{60}^+	6.40	7.05	0.48 (0.56)
$C_{59}B$	4.76	5.22	2.12 (2.39)
$C_{58}B_2$	2.54	2.80	4.34 (4.81)

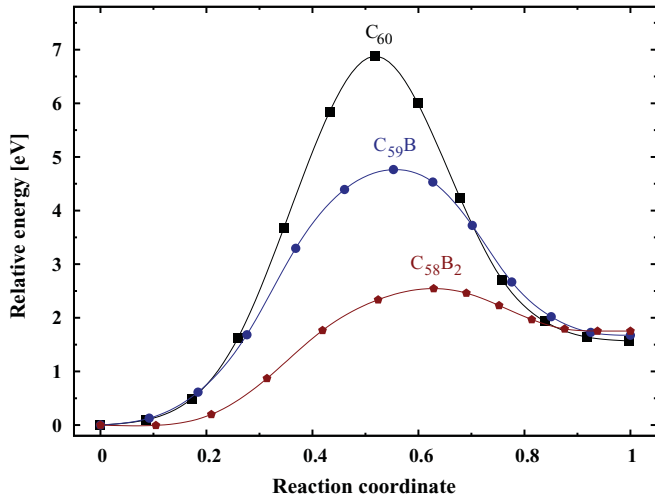


FIG. 4. (Color online) The activation energy barrier for the SW transition ($I_h \rightarrow C_{2v}$) reduces substantially for the B heterofullerenes when B is doped in the active SW sites (rotating dimer). The reverse barrier is smaller by an amount ΔE (Table I), which is similar in magnitude for all cages.

Compared to carbon nanotubes or graphitic nanostructures, the activation barrier in a fullerene is considerably less due to the strain present in the fullerene structure.²⁸ We find that the rotating C_2 unit in the transition state (TS) pops out by ~ 0.21 Å from the C_{60} surface. A similar TS was predicted previously.^{28,32,52} The bond length of the rotating C_2 unit shrinks to 1.248 Å in the TS from the corresponding bond lengths in I_h (1.399 Å) and C_{2v} (1.359 Å) symmetries.

We find that the large SW activation barrier is reduced substantially due to B doping (Table II and Fig. 4) at the active SW site. The barrier is reduced by 2.12 eV when a single C atom is replaced in the rotating dimer by B in the $C_{59}B$ heterofullerene. The reduction is comparable in magnitude with the cases where an extra carbon is strategically placed in the regions of paired pentagons² or is catalyzed by hydrogen.³³ In contrast, the endohedral metal doping has a relatively

smaller effect where the barrier is found to reduce by only 0.80 eV for La doping.²⁷ As we discussed earlier, the fact that $C_{59}B$ develops a (doublet) spin moment, we recalculated the activation barrier including spin polarization. We find that the spin-polarized activation barrier (4.67 eV) is only slightly lower than the non-spin-polarized calculation (4.76 eV).

Similar to $C_{59}B$, the activation barrier becomes lower in the singly charged fullerene C_{60}^+ compared to the neutral C_{60} . Although $C_{59}B$ is isoelectronic with C_{60}^+ , the quantitative reduction in the activation barrier is much higher for $C_{59}B$ (2.12 eV) compared to C_{60}^+ (0.48 eV). The doped B not only introduces a localized hole, but also introduces a substantial local strain. The active C-B bonds are much larger [Fig. 2(b)] and weaker compared to the C-C bonds, and thus, the activation barrier is much lower for the case of B doping.

The activation barrier is further reduced to 2.54 eV (Table II and Fig. 4) when both C atoms in the rotating dimer are replaced with B atoms for the $C_{58}B_2$ heterofullerene. Compared to pristine C_{60} , a total reduction of 4.34 eV is obtained, which is the maximum reported to date.

We find that the structure corresponding to the saddle point for all cages has only one vibrational mode with an imaginary frequency. This confirms that the obtained saddle points are indeed true first-order transition states. Frequency of the imaginary mode decreases with subsequent B doping (962, 377, and 167 cm^{-1} for C_{60} , $C_{59}B$, and $C_{58}B_2$, respectively). Thus, the variation in energy along the reaction path becomes slower, i.e., the NEB curve gets flatter, with the introduction of boron (Fig. 4).

To confirm the trend observed in the activation barrier, we have recalculated the same using an HSE06.⁵³ Although the PBE functional underestimates the activation barrier, the qualitative trend is found to be the same with the HSE06 functional (Table II). HSE06 activation barriers are calculated using the PBE reaction path and performing a single-point calculation on each intermediate image.

The origin of reduction in the SW activation barrier can be explained in terms of changes in bond strength, charge density, and phonon spectra, which point toward bond

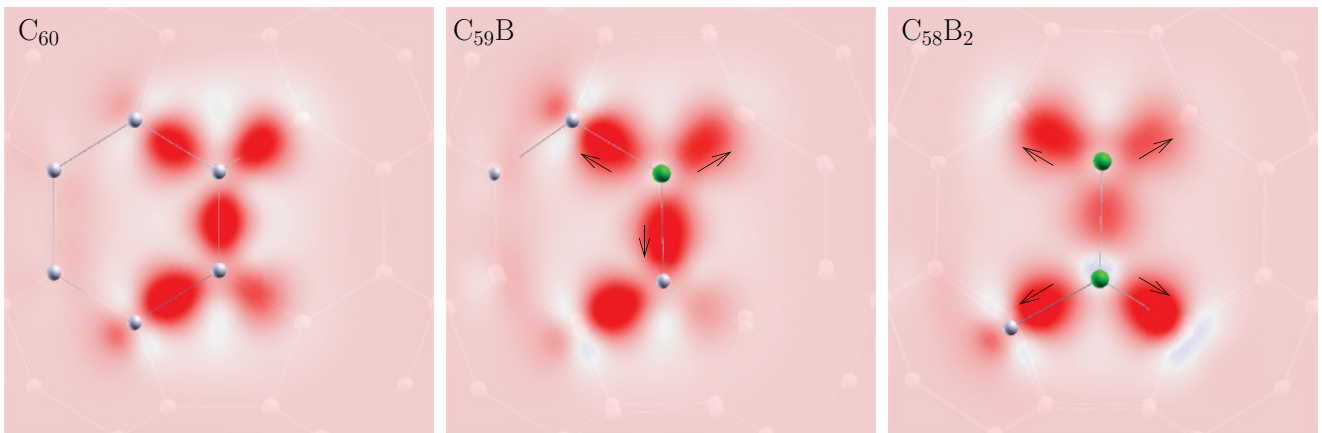


FIG. 5. (Color online) Bonding charge densities $\Delta\rho$ for pristine C_{60} , single, and double B-doped heterofullerenes. The B atoms are shown in green. The $\Delta\rho$ for a particular cage is calculated as $\Delta\rho = \rho^{\text{tot}}(\mathbf{r}) - \rho^{C_{58}}(\mathbf{r}) - \rho^X(\mathbf{r}) - \rho^Y(\mathbf{r})$, where X - Y represents the rotating C-C, C-B, and B-B dimers for C_{60} , $C_{59}B$, and $C_{59}B_2$ structures, respectively. For pristine C_{60} , the charge accumulation centers (red) appear at the middle of the bond, which indicate covalent C-C bonds. In contrast, due to B doping, the charge accumulation centers significantly shift toward the C atoms (shown with the arrows) indicating the ionic C-B character.

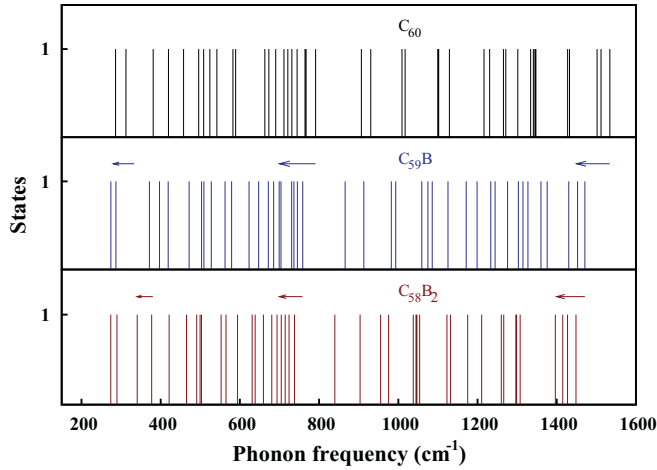


FIG. 6. (Color online) Phonons for the 14-atom pyracyclene around the rotating dimer are shown for I_h symmetry. Due to B-doping, phonons shift toward lower frequencies, which indicate bond weakening.

weakening at and around the rotating dimer. First, we calculate C-C, C-B, and B-B bond strengths in pristine C_{60} , $C_{59}B$, and $C_{58}B_2$, respectively, which can be calculated approximately using the following expressions:

$$\begin{aligned} E_{C-C} &= E_{C_{60}}^{\text{tot}}/90, \\ E_{C-B} &= [E_{C_{59}B}^{\text{tot}} - 87 \times E_{C-C}]/3, \\ E_{B-B} &= [E_{C_{58}B_2}^{\text{tot}} - 85 \times E_{C-C} - 4 \times E_{C-B}], \end{aligned} \quad (1)$$

where E^{tot} represents the total binding energy of the respective structure. We find that E_{C-C} (5.87 eV) $>$ E_{C-B} (4.74 eV) $>$ E_{B-B} (3.75 eV). Due to these weaker C-B bonds around the rotating dimer, the SW rotation becomes easier for the heterofullerenes. We further notice that the amount of reduction is related to the reduction in bond strength as $\delta E_a = n[E_{C-C} - E_{C-B}]$, where n is the number of C-B bonds involved in the SW transition for $C_{59}B$ (two) and $C_{58}B_2$ (four) heterofullerenes.

Bonding charge-density analysis (Fig. 5) also qualitatively points toward softening of the bonds that are involved in the SW process. Figure 5 shows the bonding charge densities for pristine C_{60} and B-doped heterofullerenes. For C_{60} , the C-C bonding is completely covalent i.e., the bonding charge accumulates at the centers of the bond. This picture deviates for B-doped cases, where the charge accumulation centers move toward the C atom for C-B bonds, imparting ionic character to the C-B bonds. Thus, the C-C rotation is increasingly easier for $C_{59}B$ and $C_{58}B_2$ heterofullerenes. Also, the bonding character can be understood quantitatively from Bader charge analysis,⁵⁴ which reveals that each B atom loses an $\sim 1|e|$ charge to the neighboring C atoms, which also indicate the deviation from perfect covalent character.

Next, we turn our attention to the phonon frequencies calculated at the Γ point. It is reasonable to assume that the atoms around the rotating dimer are mostly affected due to B doping and SW rotation. Thus, we considered the 14-atom pyracyclene ring around the rotating bond to calculate the normal vibrational modes. This significantly reduces the size of the Hessian matrix (from 180×180 for the full cluster

to 42×42 for the pyracyclene ring) to calculate phonon frequencies. Due to B doping, phonon frequencies gradually shift to the lower frequencies (Fig. 6). This indicates that the bonds get softer as phonon frequency (ν) is related to bond stiffness (k), $\nu \propto \sqrt{k}$. The observed softening in phonon frequencies arises due to two factors. First, the C-B and B-B bonds are longer and are weaker compared to the C-C bonds, as pointed out earlier. Additionally, the C-C bonds around the rotating unit also get elongated due to the substantial strain introduced by B doping, and thus, get weakened. The rotation of the bond is easier in such a softer environment, which eventually reduces the SW activation barrier.

C. Reaction rate and characteristic time scale

At temperatures well below the melting point, the harmonic approximation to transition state theory (HTST) can be applied to study the reaction rate or characteristic time scale associated with the reaction. The reaction rate can be expressed in terms of energy and normal mode frequencies at the saddle point and initial state,⁵⁵

$$k^{\text{HTST}} = \frac{\prod_i^{3N} \nu_i^I}{\prod_i^{3N-1} \nu_i^{\text{TS}}} e^{-(E_a/k_B T)}, \quad (2)$$

where $E_a = (E^{\text{TS}} - E^I)$ is the activation energy with E^I (E^{TS}) being the energy corresponding to the initial (transition) state and ν_i are the corresponding normal mode frequencies. Within the harmonic approximation, the entropic effect to the reaction rate is included in the prefactor involving phonon frequencies calculated at zero temperature. The first-order transition state is characterized by one imaginary phonon, which is excluded for the transition state. To calculate the prefactor, we have considered only the normal modes corresponding to the 14-atom pyracyclene ring around the rotating dimer. The characteristic time scale associated with a given reaction can be calculated from the knowledge of reaction rate k^{HTST} as $\tau = 1/k^{\text{HTST}}$. Figure 7 shows the characteristic time required for a single $I_h \rightarrow C_{2v}$ SW transition plotted as a function

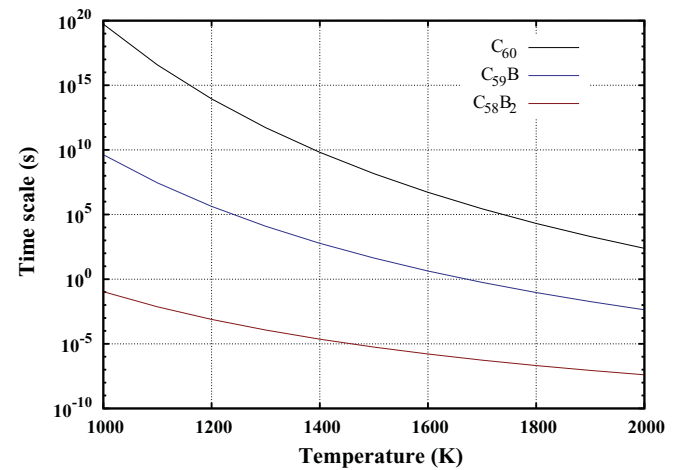


FIG. 7. (Color online) The $I_h \rightarrow C_{2v}$ transition (reaction) rate, and thus, the characteristic time scale for the corresponding transition has Arrhenius dependence on temperature and activation energy. Subsequent B doping in the rotating dimer reduces the characteristic time scale enormously via a decrease in the activation barrier.

of temperature. The characteristic time scale, measured in seconds, differs by 10^{10} – 10^6 due to subsequent B doping in the temperature range of 1000–2000 K. For example, at 1700 K, a single SW bond rotation event takes place in ~ 10 days for pristine C_{60} . In contrast, at the same temperature, the process is enormously accelerated and requires only about a second and a microsecond for $C_{59}B$ and $C_{58}B_2$, respectively. The reverse transition ($C_{2v} \rightarrow I_h$, which is not shown in Fig. 7) is $\exp(\Delta E/k_B T)$ times faster than the forward transition. For example, the reverse transition is 5 orders of magnitude faster for C_{60} at 1700 K.

IV. CONCLUSIONS

The SW activation barrier in pristine fullerenes is very large. It has been reported earlier that this high barrier can be reduced by $\sim 35\%$ due to the presence of an extra carbon or hydrogen.^{2,33} The present calculation shows that the presence of the substitutional boron at the active sites can become more effective in the reduction of the SW activation barrier. We show that it can be reduced substantially by $\sim 30\%$ and 60% via single and double B doping, respectively. Calculated bond strength, charge density, and phonon spectrum indicate that

the C-B bonds are softer compared to the C-C bonds. Thus, the presence of such weaker bonds around the rotating dimer is responsible for the observed reduction in the activation barrier. From a thermodynamic point of view, such a reduction in the barrier ΔE_a enormously reduces the time scale associated with the SW process. The reduction is on the order of $\exp(\Delta E_a/k_B T)$, which is 10^6 -fold (10^{12} -fold) at a temperature of 1700 K for single (double) B doping. SW defects are known to alter the chemical reactivity toward adsorbates,^{14–17} and thus, are expected to affect the proposed reversible H_2 storage properties of B heterofullerenes.^{35,36} Although we have shown the reduction in the SW activation barrier for fullerene here, a similar reduction is expected for carbon nanotubes and graphene nanostructures due to B doping, which could catalyze fusion, and the welding process necessary for nanoelectronic device applications.

ACKNOWLEDGMENTS

M.K. acknowledges the congenial hospitality of the S. N. Bose National Centre for Basic Sciences, Kolkata. S.M. acknowledges the Council of Scientific and Industrial Research, India for financial support.

*Corresponding author: mukulkab@mit.edu

¹A. Stone and D. Wales, *Chem. Phys. Lett.* **128**, 501 (1986); D. J. Wales, M. A. Miller, and T. R. Walsh, *Nature (London)* **394**, 758 (1998).

²B. R. Eggen, M. I. Heggie, G. Jungnickel, C. D. Latham, R. Jones, and P. R. Briddon, *Science* **272**, 87 (1996).

³M. Buongiorno Nardelli, B. I. Yakobson, and J. Bernholc, *Phys. Rev. Lett.* **81**, 4656 (1998); *Phys. Rev. B* **57**, R4277 (1998).

⁴G. G. Samsonidze, G. G. Samsonidze, and B. I. Yakobson, *Phys. Rev. Lett.* **88**, 065501 (2002).

⁵Y. Miyamoto, A. Rubio, S. Berber, M. Yoon, and D. Tománek, *Phys. Rev. B* **69**, 121413 (2004).

⁶Y.-H. Kim, I.-H. Lee, K. J. Chang, and S. Lee, *Phys. Rev. Lett.* **90**, 065501 (2003); Y. Zhao, B. I. Yakobson, and R. E. Smalley, *ibid.* **88**, 185501 (2002).

⁷M. Yoon, S. Han, G. Kim, S. B. Lee, S. Berber, E. Osawa, J. Ihm, M. Terrones, F. Banhart, J.-C. Charlier, N. Grobert, H. Terrones, P. M. Ajayan, and D. Tománek, *Phys. Rev. Lett.* **92**, 075504 (2004).

⁸M. Ouyang, J.-L. Huang, C. L. Cheung, and C. M. Lieber, *Science* **291**, 97 (2001); V. H. Crespi, M. L. Cohen, and A. Rubio, *Phys. Rev. Lett.* **79**, 2093 (1997).

⁹E. J. Duplock, M. Scheffler, and P. J. D. Lindan, *Phys. Rev. Lett.* **92**, 225502 (2004).

¹⁰F. OuYang, B. Huang, Z. Li, J. Xiao, H. Wang, and H. Xu, *J. Phys. Chem. C* **112**, 12003 (2008).

¹¹H. Terrones and A. Mackay, *Carbon* **30**, 1251 (1992).

¹²J. Ma, D. Alfè, A. Michaelides, and E. Wang, *Phys. Rev. B* **80**, 033407 (2009).

¹³D. Ugarte, *Nature (London)* **359**, 707 (1992).

¹⁴Z. Slanina, X. Zhao, F. Uhlík, M. Ozawa, and E. Ōsawa, *J. Organomet. Chem.* **599**, 57 (2000).

¹⁵D. Tasis, N. Tagmatarchis, A. Bianco, and M. Prato, *Chem. Rev.* **106**, 1105 (2006).

¹⁶A. H. Nevidomskyy, G. Csányi, and M. C. Payne, *Phys. Rev. Lett.* **91**, 105502 (2003).

¹⁷H. F. Bettinger, *J. Phys. Chem. B* **109**, 6922 (2005).

¹⁸J. Kang, J. Bang, B. Ryu, and K. J. Chang, *Phys. Rev. B* **77**, 115453 (2008).

¹⁹D. W. Boukhvalov and M. I. Katsnelson, *Nano Lett.* **8**, 4373 (2008).

²⁰H. F. Bettinger, T. Dumitrică, G. E. Scuseria, and B. I. Yakobson, *Phys. Rev. B* **65**, 041406 (2002); W. Chen, Y. Li, G. Yu, Z. Zhou, and Z. Chen, *J. Chem. Theory Comput.* **5**, 3088 (2009).

²¹Y. Lin, T. V. Williams, W. Cao, H. E. Elsayed-Ali, and J. W. Connell, *J. Phys. Chem. C* **114**, 17434 (2010); C. Y. Won and N. R. Aluru, *J. Am. Chem. Soc.* **130**, 13649 (2008); X. Wu, J. Yang, J. G. Hou, and Q. Zhu, *J. Chem. Phys.* **124**, 054706 (2006); Y. Li, Z. Zhou, D. Golberg, Y. Bando, P. von Ragué Schleyer, and Z. Chen, *J. Phys. Chem. C* **112**, 1365 (2008); W. An, X. Wu, J. L. Yang, and X. C. Zeng, *ibid.* **111**, 14105 (2007).

²²S. Austin, P. Fowler, D. Manolopoulos, and F. Zerbetto, *Chem. Phys. Lett.* **235**, 146 (1995).

²³T. R. Walsh and D. J. Wales, *J. Chem. Phys.* **109**, 6691 (1998).

²⁴C. Xu and G. E. Scuseria, *Phys. Rev. Lett.* **72**, 669 (1994).

²⁵H. W. Kroto, *Nature (London)* **329**, 529 (1987).

²⁶S. J. Austin, P. W. Fowler, D. E. Manolopoulos, G. Orlandi, and F. Zerbetto, *J. Phys. Chem.* **99**, 8076 (1995).

²⁷W. I. Choi, G. Kim, S. Han, and J. Ihm, *Phys. Rev. B* **73**, 113406 (2006).

²⁸J.-Y. Yi and J. Bernholc, *J. Chem. Phys.* **96**, 8634 (1992).

²⁹Y.-Z. Tan, Z.-J. Liao, Z.-Z. Qian, R.-T. Chen, X. Wu, H. Liang, X. Han, F. Zhu, S.-J. Zhou, Z. Zheng, X. Lu, S.-Y. Xie, R.-B. Huang, and L.-S. Zheng, *Nature Mater.* **7**, 790 (2008).

³⁰R.-T. Chen, S.-J. Zhou, H. Liang, Z.-Z. Qian, J.-M. Li, Q. He, L. Zhang, Y.-Z. Tan, X. Han, Z.-J. Liao, W.-Z. Weng, S.-Y. Xie, R.-B. Huang, and L.-S. Zheng, *J. Phys. Chem. C* **113**, 16901 (2009).

- ³¹M. S. Dresselhaus, G. Dresselhaus, and P. C. Eklund, *Science of Fullerenes and Carbon Nanotubes* (Academic, San Diego, 1996).
- ³²H. F. Bettinger, B. I. Yakobson, and G. E. Scuseria, *J. Am. Chem. Soc.* **125**, 5572 (2003).
- ³³M. I. Heggie, C. D. Latham, R. Jones, and P. R. Briddon, in *Fullerenes: Chemistry, Physics, and New Directions VII*, edited by K. M. Kadish and R. S. Rudoff (Electrochemical Society, Pennington, NJ, 1995), pp. 1218–1223.
- ³⁴H. J. Muhr, R. Nesper, B. Schnyder, and R. Kötz, *Chem. Phys. Lett.* **249**, 399 (1996); T. Guo, C. Jin, and R. E. Smalley, *J. Phys. Chem.* **95**, 4948 (1991).
- ³⁵Y. Zhao, Y.-H. Kim, A. C. Dillon, M. J. Heben, and S. B. Zhang, *Phys. Rev. Lett.* **94**, 155504 (2005).
- ³⁶Y.-H. Kim, Y. Zhao, A. Williamson, M. J. Heben, and S. B. Zhang, *Phys. Rev. Lett.* **96**, 016102 (2006).
- ³⁷G. Kresse and J. Hafner, *Phys. Rev. B* **47**, 558 (1993); G. Kresse and J. Furthmüller, *ibid.* **54**, 11169 (1996).
- ³⁸P. E. Blöchl, *Phys. Rev. B* **50**, 17953 (1994).
- ³⁹J. P. Perdew, K. Burke, and M. Ernzerhof, *Phys. Rev. Lett.* **77**, 3865 (1996).
- ⁴⁰G. Henkelman, B. P. Uberuaga, and H. Jónsson, *J. Chem. Phys.* **113**, 9901 (2000); G. Henkelman and H. Jónsson, *ibid.* **113**, 9978 (2000).
- ⁴¹M. Hser, J. Almlf, and G. E. Scuseria, *Chem. Phys. Lett.* **181**, 497 (1991).
- ⁴²W. I. F. David, R. M. Ibberson, J. C. Matthewman, K. Prassides, T. J. S. Dennis, J. P. Hare, H. W. Kroto, R. Taylor, and D. R. M. Walton, *Nature (London)* **353**, 147 (1991).
- ⁴³K. Hedberg, L. Hedberg, D. S. Bethune, C. A. Brown, H. C. Dorn, R. D. Johnson, and M. De Vries, *Science* **254**, 410 (1991).
- ⁴⁴S. Liu, Y.-J. Lu, M. M. Kappes, and J. A. Ibrs, *Science* **254**, 408 (1991).
- ⁴⁵C. S. Yannoni, P. P. Bernier, D. S. Bethune, G. Meijer, and J. R. Salem, *J. Am. Chem. Soc.* **113**, 3190 (1991).
- ⁴⁶X. Blase, C. Attacalite, and V. Olevano, *Phys. Rev. B* **83**, 115103 (2011).
- ⁴⁷I. V. Hertel, H. Steger, J. de Vries, B. Weisser, C. Menzel, B. Kamke, and W. Kamke, *Phys. Rev. Lett.* **68**, 784 (1992).
- ⁴⁸L.-S. Wang, J. Conceicao, C. Jin, and R. Smalley, *Chem. Phys. Lett.* **182**, 5 (1991).
- ⁴⁹J. D. Sau, J. B. Neaton, H. J. Choi, S. G. Louie, and M. L. Cohen, *Phys. Rev. Lett.* **101**, 026804 (2008).
- ⁵⁰E. Kaxiras and K. C. Pandey, *Phys. Rev. Lett.* **61**, 2693 (1988).
- ⁵¹T. Dumitrica and B. I. Yakobson, *Appl. Phys. Lett.* **84**, 2775 (2004).
- ⁵²R. L. Murry, D. L. Strout, G. K. Odom, and G. E. Scuseria, *Nature (London)* **366**, 665 (1993).
- ⁵³J. Heyd, G. E. Scuseria, and M. Ernzerhof, *J. Chem. Phys.* **118**, 8207 (2003); A. F. Izmaylov, G. E. Scuseria, and M. J. Frisch, *ibid.* **125**, 104103 (2006).
- ⁵⁴R. F. W. Bader, *Atoms in Molecules-A Quantum Theory* (Oxford University Press, Oxford, 1990); G. Henkelman, A. Arnaldsson, and H. Jnsson, *Comput. Mater. Sci.* **36**, 354 (2006).
- ⁵⁵G. H. Vineyard, *J. Phys. Chem. Solids* **3**, 121 (1957).